

N-doped Fe@CNT for combined RWGS/FT CO₂ hydrogenation

SUPPORTING INFORMATION

Authors: David L. Williamson, Carmelo Herdes, Laura Torrente-Murciano, Matthew D. Jones and Davide Mattia

This document consists of:

Pages: 11

Figures: 11

Tables: 3

Materials composition & justification of activation conditions

Table S1 Surface compositions of Fe@NCNT as-synthesized, after activation, and after CO₂ conversion testing, as determined by XPS analysis.

Sample		Composition [At. %]			
		C	N	O	Fe
Synthesized	Fe@NCNTs	94.3	2.7	2.8	0.3
Activated	Fe@NCNTs	88.9	2.3	7.4	1.5
Post-reaction	Fe@NCNTs	91.0	1.2	4.1	0.8

Catalyst Fe@NCNT composition and nitrogen doping was determined via XPS, as can be seen in Table S1.

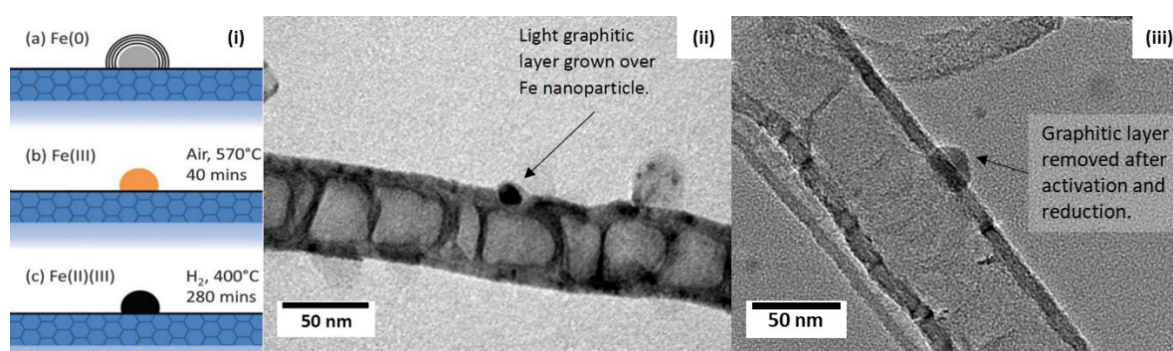


Figure S1. (i) Schematic illustrating the oxidation states of the iron nanoparticles in Fe@CNTs (a) as synthesised, (b) following thermal activation, and (c) following reduction prior to catalytic testing. Removal of the protective graphitic layer during the activation step is clearly communicated. (ii) TEM micrograph of freshly synthesized Fe@NCNT clearly exhibiting the presence of a similar graphitic layer over the iron nanoparticle.¹ (iii) TEM micrograph of activated and reduced Fe@NCNT illustrating the removal of the graphitic layer during activation and a similar sample morphology after reduction.

It has been previously determined that the catalytic iron particles in Fe@CNT-type materials remain obscured beneath a thin graphitic carbon layer directly after synthesis. This layer prevents them from participating CO₂ hydrogenation must therefore be removed via calcination in air to activate the catalyst prior to CO₂ hydrogenation. Activation at 570 °C for 40 minutes has been shown to sufficiently remove the graphitic layer in Fe@CNT, resulting in ca. 1 at. % iron exposure as determined by XPS.¹ However, due to lattice defects that form as a result of nitrogen doping in Fe@NCNT, their thermal stability is decreased and milder activation conditions must be applied to expose similar levels of iron without destroying the catalyst.

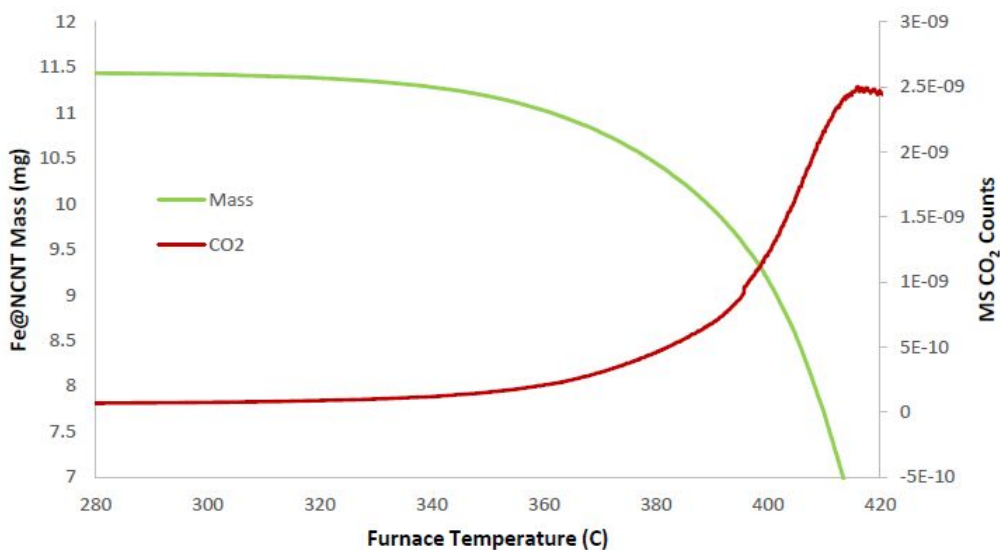


Figure S2. Mass loss and CO₂ counts of Fe@NCNT from 280 – 420 °C, as measured via TG-MS.

TG-MS, TEM and XPS were used to determine suitable activation conditions for the Fe@NCNT. The decomposition of Fe@NCNT was monitored in air via TG-MS in an attempt to identify a distinct decomposition temperature for the graphitic layer prior to the onset of decomposition for the NCNT support material. No distinct decomposition mode was detected for the graphitic layer. This suggests that either the decomposition of the graphitic layer is too small to be detectable, or the graphitic layer has a similar thermal stability to the NCNT support and must therefore be removed through a quick activation procedure that serves to expose the iron particles before the NCNT support can be significantly damaged.

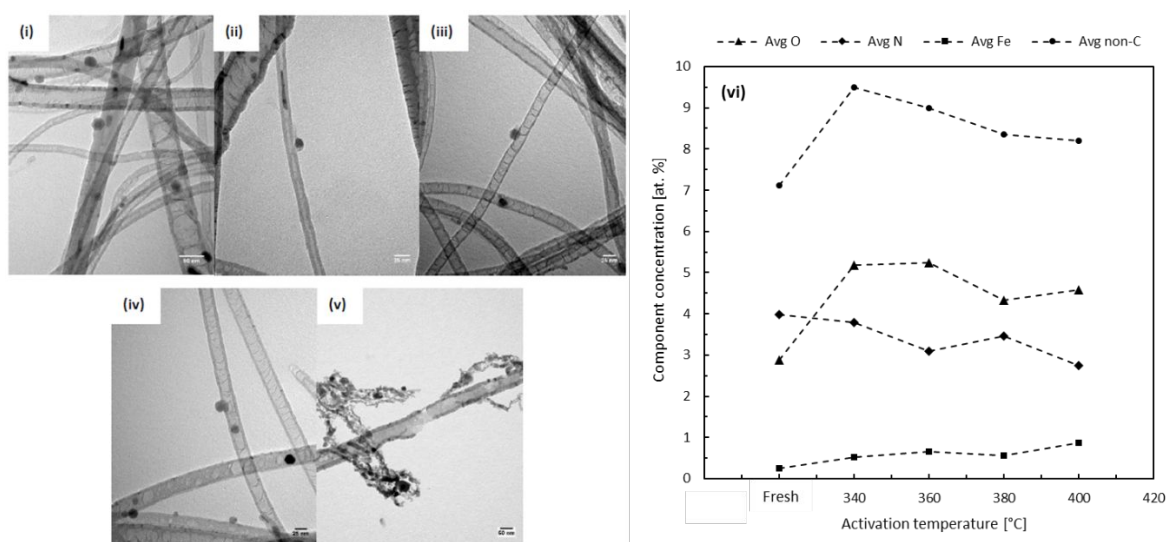


Figure S3. TEM micrographs of Fe@NCNT activated in air for 1 hour at (i) 340 °C, (ii) 360 °C, (iii) 380 °C, (iv) 400 °C, and (v) 420 °C. (vi) Effect of activation temperature on catalyst composition as determined by XPS.

TEM micrographs were subsequently corroborated with XPS analysis of Fe@NCNT at different activation temperatures to monitor iron exposure and the integrity of the NCNT support after a 1 hour activation procedure. Activation at 400 °C was determined to be suitable, as this resulted in ca.

1 at. % of exposed iron (similar to Fe@NCNT activated at 570 °C), while keeping the NCNT support material intact. Activation at 420 °C was observed to significantly damage the NCNT support.

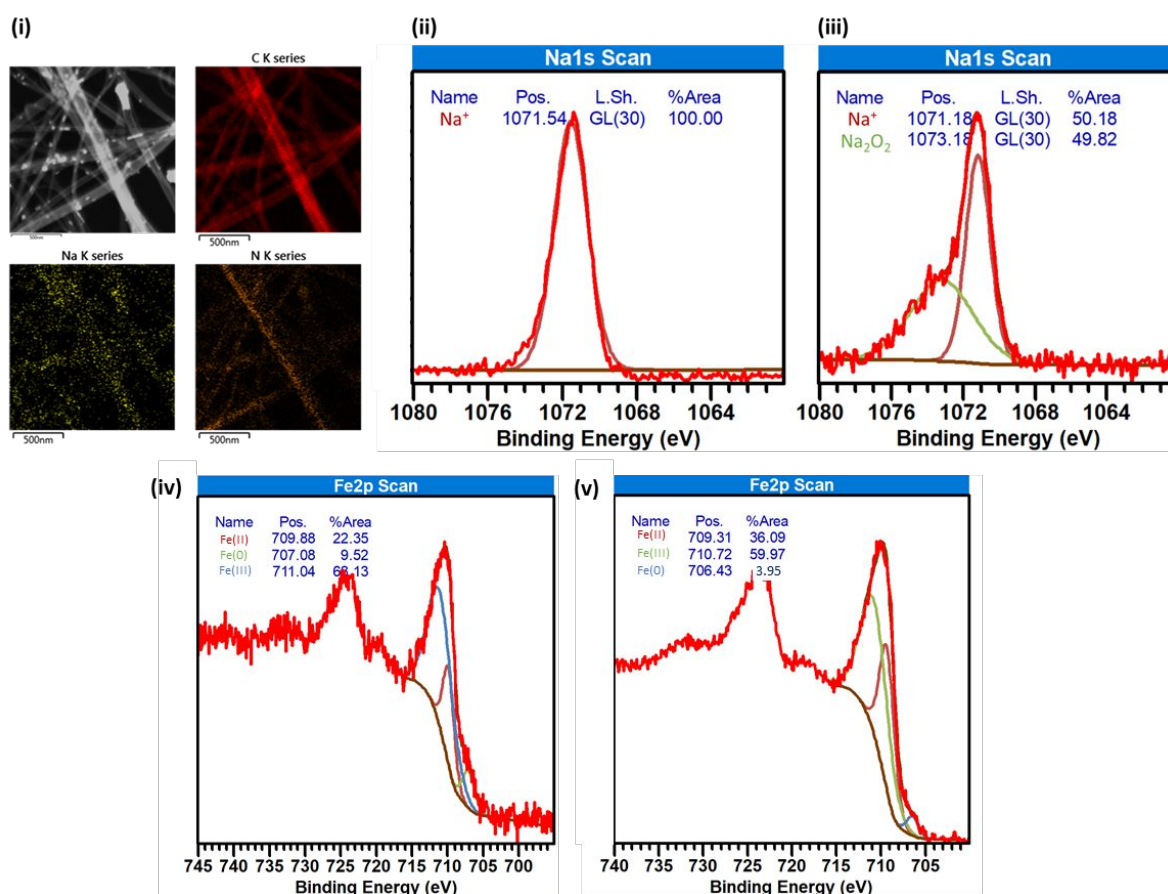


Figure S4. (i) EDS maps of Na-Fe@NCNT displaying uniform sodium dispersion along the NCNT tube exterior after activation at 400 °C in air for 1 hour. XPS Na 1s regions of Na-Fe@NCNT (ii) directly after sodium doping and (iii) after activation at 400 °C in air for 1 hour. XPS Fe 2p regions of (iv) Na-Fe@NCNT and (v) Fe@NCNT after activation at 400 °C in air for 1 hour.

EDS characterisation was used to determine the location of sodium in the Na-Fe@NCNT sample. Uniform dispersion of sodium is visible along the exterior of the NCNT tubes in small point clusters suggesting obfuscation of nitrogen sites due to their greater electron density through Na⁺ coordination. Nitrogen and carbon maps provide a greater signal-to-noise ratio due to their presence throughout the bulk of the tubes, which is still detected by EDS despite having no effect on the catalytic process at the interface of the catalyst. Comparatively, only a small amount of Na is present in the sample (0.5 wt. % doped via wet impregnation). However, this Na is present exclusively at the catalyst surface where its interactions with surface nitrogen sites has a significant effect on catalytic performance.

Deposition of Na⁺ to obscure surface nitrogen sites is further supported by XPS analysis. After initial Na doping via wet impregnation, all Na in the sample exists as Na⁺, evidenced by a single peak at 1071.5 eV. In previous publications, Beard has shown that pure Na(i) in the form of fresh cleaved single crystal NaCl exhibits a characteristic Na 1s peak at 1071.1 eV,² while Wu et al. have shown that this peak shifts to 1072.0 eV for Na⁺ stabilised by the presence of a negatively charged counterion.³ The Na⁺ peak shift to 1071.5 eV for Na-Fe@NCNT following wet impregnation can therefore be taken as evidence of weaker N^{δ-} → Na⁺ interactions between nitrogen sites and their obscuring Na⁺

species. Following activation at 400 °C in air for 1 hour, ca. 50% of the Na⁺ is converted to Na₂O₂ (1073.2 eV), while half remains stabilised as Na(i) (1071.2 eV).⁴ Fe 2p regions of Na-Fe@NCNT and Fe@NCNT after activation at 400 °C in air for 1 hour show similar iron compositions across both samples. Na-Fe@NCNT display a greater presence of both Fe(III) and Fe(0), while Fe@NCNT display a greater presence of Fe(II). These differences in composition are likely affected by variance in the samples and margin of error in the XPS measurement rather than electronic perturbations in the iron caused by Na doping. It is unlikely that the Na-Fe@NCNT would possess the greatest concentrations of both the most and least reduced metals species if Na doping significantly enhanced or inhibited the reducibility of the iron.

Computational methodology

Here a molecular dynamics (MD) simulation approach mimics i) the pre-reaction and ii) the post-reaction adsorption stages of the system at given experimental compositions, in order to isolate and quantify the effect of nitrogen doping of the suggested catalyst by common statistical molecular thermodynamics properties such as total and pair energy landscape at isothermal adsorption equilibrium conditions, aiming to shed light on the proposed reaction mechanism.

Molecular models

All species were modelled with available full atomistic force fields, specifically, iron(III) oxide nanoparticles (Fe₂O₃) were simulated via a Lennard-Jones (LJ) potential with constant coulombic charges,⁵ carbon nanotubes (CNTs) by LJ parameters derived for small diameter CNTs from van der Waals density functional calculations,⁶ nitrogen doping atoms followed a model for surface heterogeneities on kerogen for gas storage⁷ a diatomic hydrogen model used for adsorption (and desorption) molecular dynamics studies on graphite,⁸ a simple three-site model of carbon dioxide (CO₂) molecules previously validated for its pure vapour-liquid equilibrium and critical properties predictions,⁹ a two site model of carbon oxide, used to simulate its relaxation process at fullerene environment, was selected,¹⁰ and water molecules were represented by the well-known SPC/E model from Berendsen.¹¹ Models⁵⁻¹¹ were used without further modifications from the originals, for predictive aim. Cross-interactions followed the common Lorentz-Berthelot combining rules with the exception of the CO₂ model where optimised parameters exist for $\sigma_{C-O}=0.2892$ nm and $\epsilon_{C-O}/k_B=47.588$ K.⁸ The implemented molecular parameters are summarized in Table S2.

Table S2. Lennard-Jones potential and coulombic parameters summary for studied species.

	Atom (Molecule)	σ [nm]	ϵ/k_B [K]	q [e]	Reference
Catalyst	Fe (Fe₂O₃)	0.220000	42.749	0.7710	v
	O (Fe₂O₃)	0.296000	85.497	-0.5140	
	C (CNT)	0.351400	35.914	-	vi
	N (NCNT)	0.390000	48.320	-	vii
Reactants	H (H₂)[*]	0.263984	27.655	-	viii
	C (CO₂)^{**}	0.275700	28.129	0.6512	ix
	O (CO₂)	0.303300	80.507	-0.3256	
Products	C (CO)^{***}	0.355000	37.152	0.0223	x

	O (CO)	<i>0.295000</i>	<i>61.579</i>	<i>-0.0223</i>	
	H (H₂O)[§]	-	-	<i>0.4238</i>	<i>xi</i>
	O (H₂O)	<i>0.355330</i>	<i>78.202</i>	<i>-0.8476</i>	

* H-H interatomic distance 0.07414 nm.

** C-O interatomic distance 0.1149 nm.

*** C-O interatomic distance 0.1128 nm.

§ H-O interatomic distance 0.1 nm; H-O-H angle 109.47 deg.

Simulation details

MD simulations were performed under the NVT, NPT and NPzzAT ensembles, at common wet laboratory conditions, with pressure and temperature maintained via the Parrinello-Rahman barostat and Nose-Hoover thermostat respectively, meanwhile, the number of molecules in each studied system was kept constant and followed the needed experimental composition. MD simulations were carried out using GROMACS v5.1. Periodic boundary conditions were applied to the simulation cells. A simple cut-off radius of 1.2 nm was applied. Long-range interactions were calculated by standard PME method. The LINCS algorithm was employed to constrain the molecular bonds. The time resolution of the equations of motions was set to 2 fs. The different systems were monitored until the relevant properties (e.g. density, total energy, etc.) attained equilibrium, afterwards, production runs were extended at least 2 ns for the reported averages.

Iron(III) Fe₂O₃ nanoparticles simulated synthesis

An initial NVT simulation cell of 40 nm side containing 200 iron atoms and 300 oxygen atoms was equilibrated at 900K, see figure S5a, the clustering of Fe₂O₃ molecules was attained after 2 ns see figure S5b.

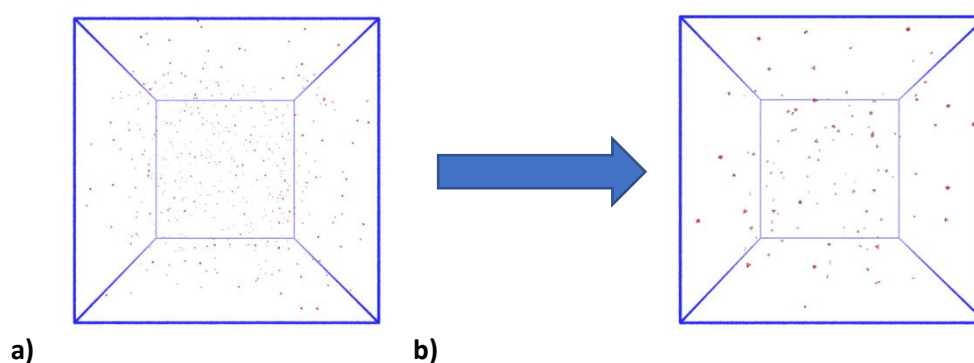


Figure S5. a) Initial and b) equilibrated NVT simulation cell for Fe₂O₃ clustering.

Afterwards, the Fe₂O₃ molecules were subject to isothermal compression via an NPT ensemble at high pressure, 100 bar, down to a cubic box of ca. 3 nm, see figure S6a. This system was then duplicated in all directions to form a cubic box of ca. 6 nm, hosting 1600 Fe and 2400 O atoms, see figure S6b.

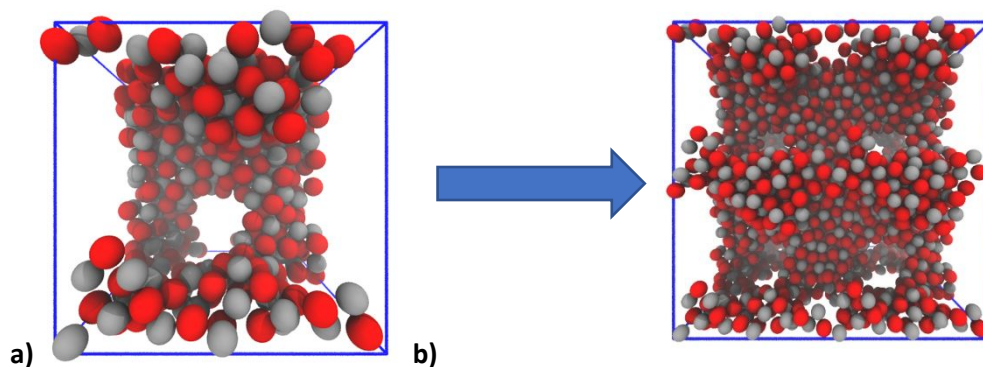


Figure S6. a) NPT isothermal compression of Fe_2O_3 molecules and b) duplicated simulation cell of 800 Fe_2O_3 molecules.

To promote the nanoparticle formation the boundary of the system was expanded three times in each direction, see Figure S7a, under NVT conditions. Almost immediately, an Fe_2O_3 nanoparticle of ~ 2.5 nm was created and isolated for further studies, see Figure S7b.

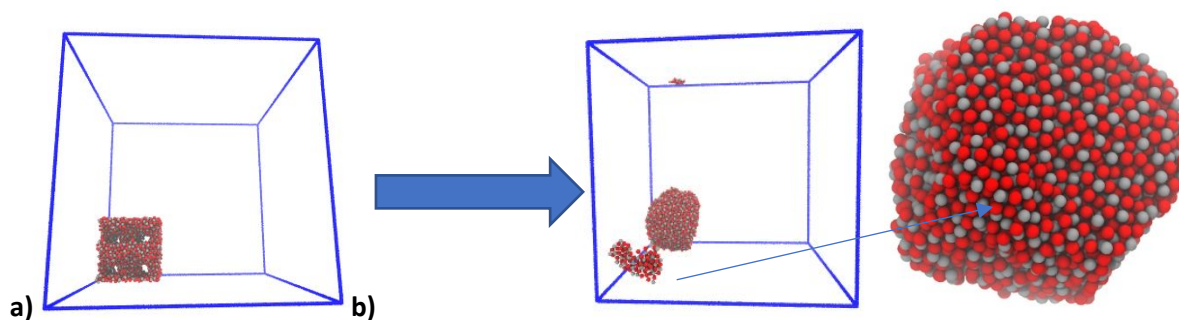


Figure S7. a) Expanded boundary simulation cell to promote a b) Fe_2O_3 nanoparticle of ~ 2.5 nm.

Iron(III) Fe_2O_3 nanoparticles simulated deposition onto CNT

The attained Fe_2O_3 nanoparticle was placed in a cubic (30 nm side length) NVT vacuum cell at 25 °C, containing a single-walled armchair CNT(100,100), 13.6 nm in diameter, of 40 000 carbon atoms. The CNT central axis was oriented perpendicular to the z-axis of the simulation cell and its position was kept constant during the whole simulation meanwhile the Fe_2O_3 nanoparticle was allowed to move. Snapshots of the deposition sequence can be seen in Figure S8.

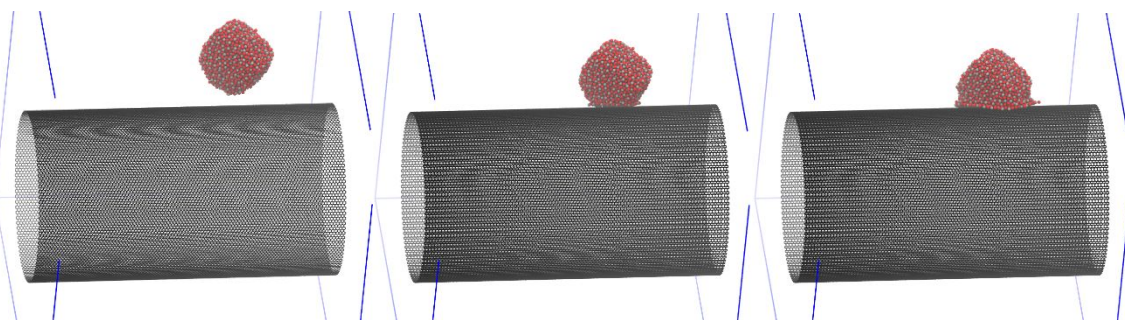


Figure S8. Fe₂O₃ nanoparticle deposition onto CNT sequence.

Adsorption behaviour of H₂:CO₂ (3:1 composition) on CNT and NCNT

950 CO₂ and 2850 H₂ molecules were randomly inserted into the last simulation cell of the deposition sequence in Figure 8. Before the adsorption studies, the NPzzAT ensemble was then used to correct the cell volume, by changing the z-length of the box, in order to attain the desired pressure level of 15 bar at 370 °C, see Figure S9.

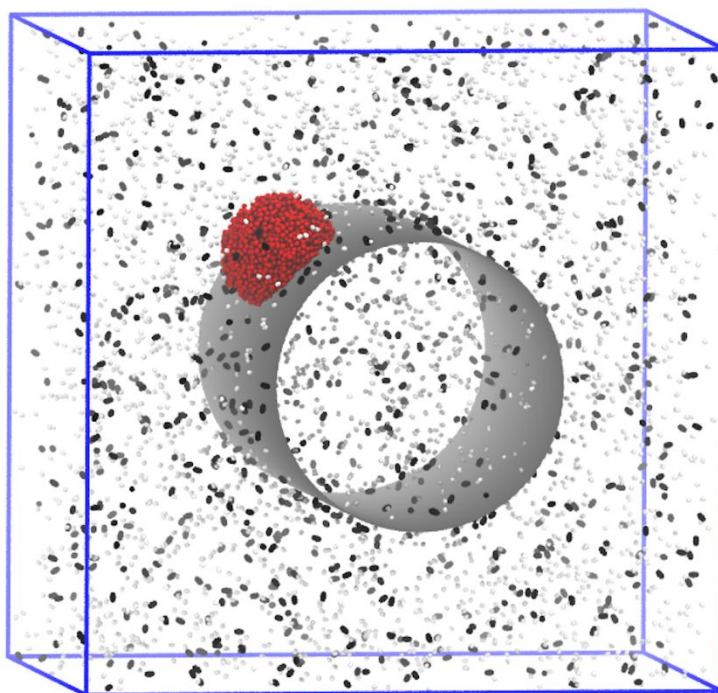


Figure S9. Fe₂O₃CNT loaded simulation cell with H₂:CO₂ 3:1 ratio at 15 bar and 370 °C. The CNT is depicted as a smooth grey surface, H₂, CO₂, and Fe₂O₃ molecules are coloured white, black and red, respectively, for the sake of contrast.

The loaded simulation cell (see Figure S9) was allowed then to equilibrate under the NVT ensemble (once the pressure level was achieved, via NPzzAT, at ~25 nm in the z-length keeping the xy area at 30x30 nm²).

The nitrogen doping procedure was simulated by randomly replacing 3% of the carbon atoms of the CNT by nitrogen atoms, see Figure S10.

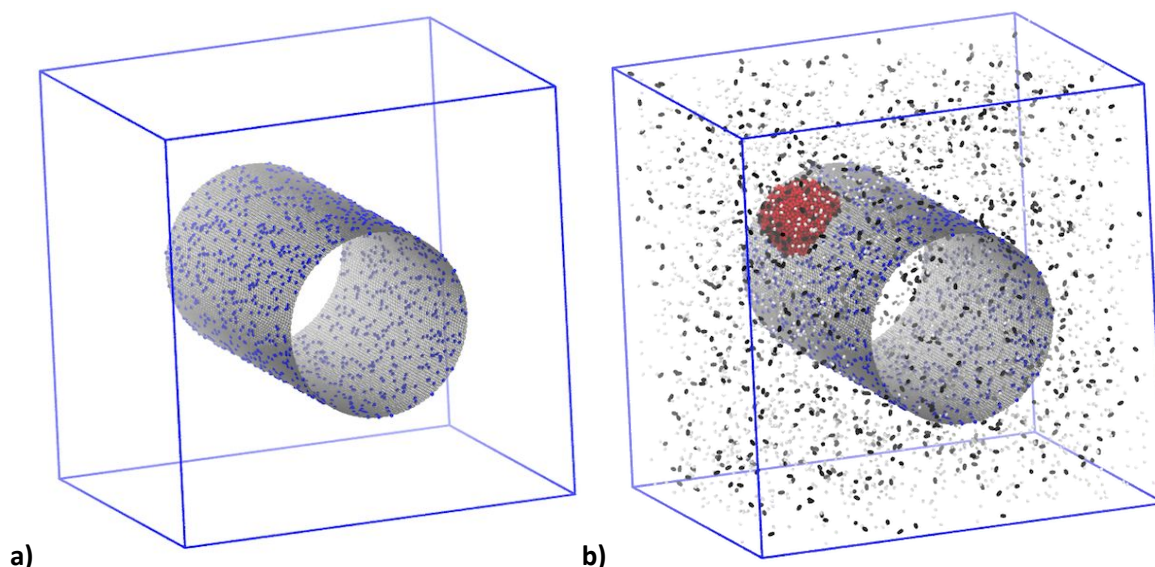


Figure S10. a) $\text{Fe}_2\text{O}_3\text{NCNT}$ obtained by random substitution of 3% of carbon atoms by nitrogen atoms. b) Nitrogen-doped cell presenting all atoms as the loaded cell in Figure S9.

Analogous, starting points, adsorption studies for both systems were performed to isolate the effect of nitrogen doping via total and relevant pair energies calculation obtained after equilibration as average values from production runs of at least 2 ns.

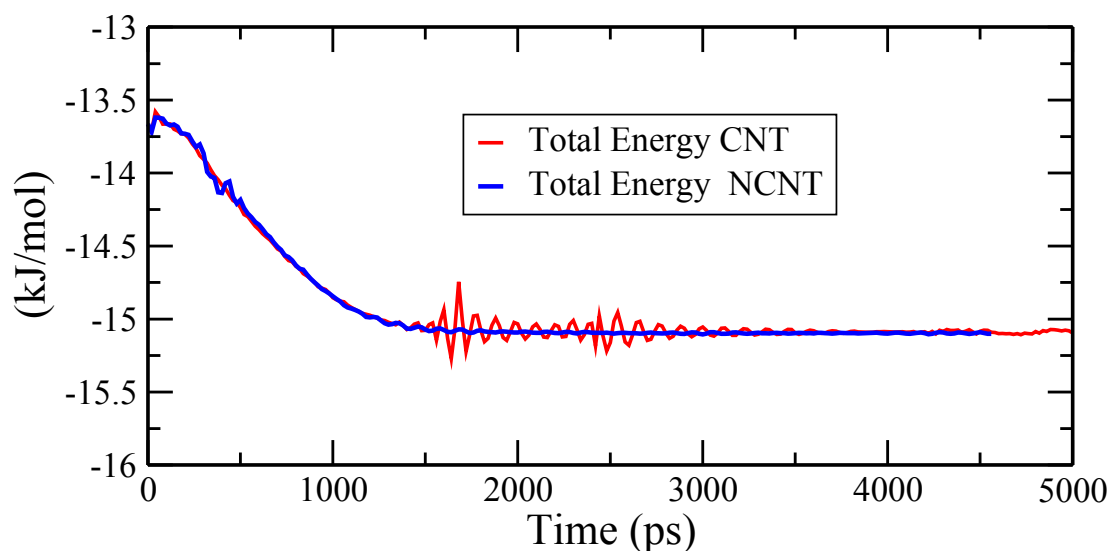


Figure S11. Total energy (potential + kinetic) comparison between $\text{Fe}_2\text{O}_3\text{CNT}$ (red) and $\text{Fe}_2\text{O}_3\text{NCNT}$ (blue).

At first glance, see Figure S11, both systems tend to equilibrate at 15.090 kJ/mol, however, the NCNT seems to have a catalytic and smoothing effect over the adsorption of the species equilibrating at ~ 1.5 ns meanwhile the CNT system needs ~ 3.5 ns to do so. The energy percentage contribution to the total potential energy, from relevant pair interactions (LJ + Coulombic), has been reported in Table S3 for each system.

Table S3. Percentage contribution to the potential energy (LJ + coulombic) of selected pairs, before reaction.

Pair interaction	%	
	CNT	NCNT
CO₂ - Catalyst	4.10	5.31
H₂ - Catalyst	2.84	3.06
H₂ - CO₂	1.19	1.10
CO₂ - CO₂	1.22	1.14
H₂ - H₂	1.15	1.09

Under the accuracy of the simulation (estimated error of ± 0.006 kJ/mol), the total energy of both systems is identical. However, in comparison to the CNT, the NCNT promoted slightly fewer interactions between the fluids (i.e. pure H₂, pure CO₂ and their cross interactions), while increasing reactants contact with the catalyst. Snapshots of each system can be seen in Figure 6 in the main manuscript for further spatial considerations. As expected from the energy landscape results, both systems present very similar layouts with hydrogen molecules adsorbed preferentially into the iron oxide nanoparticle surrounded by a skirt composed of hydrogen and carbon dioxide molecules absorbed in the carbon nanotube. Another interesting feature is the development of carbon dioxide islands with a hydrogen coastal-line on the surface of the carbon nanotube with and without nitrogen, it is worth noticing that these islands remained static after their formation for the entire length of the simulations.

References

- O'Byrne, J. P.; Owen, R. E.; Minett, D. R.; Pascu, S. I.; Plucinski, P. K.; Jones, M. D.; Mattia, D., High CO₂ and CO conversion to hydrocarbons using bridged Fe nanoparticles on carbon nanotubes. *Catal. Sci. Technol.* **2013**, *3* (5), 1202-1207.
- Beard, B. C., Fresh Cleaved Single Crystal NaCl, XPS Spectra, Al Source. *Surface Science Spectra* **1993**, *2* (2), 91-96.
- Wu, S.; Wang, W.; Li, M.; Cao, L.; Lyu, F.; Yang, M.; Wang, Z.; Shi, Y.; Nan, B.; Yu, S.; Sun, Z.; Liu, Y.; Lu, Z., Highly durable organic electrode for sodium-ion batteries via a stabilized α -C radical intermediate. *Nat. Commun.* **2016**, *7*, 13318.
- Takanabe, K.; Khan, A. M.; Tang, Y.; Nguyen, L.; Ziani, A.; Jacobs, B. W.; Elbaz, A. M.; Sarathy, S. M.; Tao, F., Integrated In Situ Characterization of a Molten Salt Catalyst Surface: Evidence of Sodium Peroxide and Hydroxyl Radical Formation. *Angewandte Chemie International Edition* **2017**, *56* (35), 10403-10407.
- Berro, H.; Fillot, N.; Vergne, P., Molecular dynamics simulation of surface energy and ZDDP effects on friction in nano-scale lubricated contacts. *Tribology International* **2010**, *43* (10), 1811-1822.
- Kaukonen, M.; Gulans, A.; Havu, P.; Kauppinen, E., Lennard-Jones parameters for small diameter carbon nanotubes and water for molecular mechanics simulations from van der Waals density functional calculations. *J. Comput. Chem.* **2012**, *33* (6), 652-658.
- Cristancho, D.; Akkutlu, I. Y.; Criscenti, L. J.; Wang, Y., Gas Storage in Model Kerogen Pores with Surface Heterogeneities. In *SPE Europe featured at 78th EAGE Conference and Exhibition*, Society of Petroleum Engineers: Vienna, Austria, 2016; p 16.

8. Simon, J. M.; Haas, O. E.; Kjelstrup, S., Adsorption and Desorption of H₂ on Graphite by Molecular Dynamics Simulations. *The Journal of Physical Chemistry C* **2010**, *114* (22), 10212-10220.
9. Harris, J. G.; Yung, K. H., Carbon dioxide's liquid-vapor coexistence curve and critical properties as predicted by a simple molecular model. *The Journal of Physical Chemistry* **1995**, *99* (31), 12021-12024.
10. Pałucha, S.; Gburski, Z.; Biesiada, J., A molecular dynamics study of fullerene-carbon monoxide mixture. *J. Mol. Struct.* **2004**, *704* (1), 269-273.
11. Berendsen, H.; Grigera, J.; Straatsma, T., The missing term in effective pair potentials. *J. Phys. Chem.* **1987**, *91* (24), 6269-6271.